Allowed and forbidden transitions in artificial hydrogen and helium atoms

Toshimasa Fujisawa*, David Guy Austing*,†, Yasuhiro Tokura*, Yoshiro Hirayama*,‡ & Seigo Tarucha*,§,‖
*NTT Basic Research Laboratories, NTT Corporation, 3-1 Morinosato-Wakamiya, Atsugi, 243-0198, Japan
†Institute for Microstructual Sciences M23A, National Research Council of Canada, Ottawa, Ontario K1A 0R6, Canada
‡CREST, 4-1-8 Honmachi, Kawaguchi, 331-0012, Japan
§University of Tokyo, Bunkyo-ku, Tokyo, 113-0033, Japan
‖ERATO Mesoscopic Correlation Project, 3-1 Morinosato-Wakamiya, Atsugi, 243-0198, Japan

The strength of radiative transitions in atoms is governed by selection rules[1]. Spectroscopic studies of allowed transitions in hydrogen and helium provided crucial evidence for the Bohr's model of an atom. "Forbidden" transitions, which are actually allowed by higher-order processes or other mechanisms, indicate how well the quantum numbers describe the system. We apply these tests to the quantum states in semiconductor quantum dots (QDs), which are regarded as artificial atoms. Electrons in a QD occupy quantized states in the same manner as electrons in real atoms[2–5]. However, unlike real atoms, the confinement potential of the QD is anisotropic, and the electrons can easily couple with *phonons* of the material[6]. Understanding the selection rules for such QDs is an important issue for the manipulation of quantum states. Here we investigate allowed and forbidden transitions for phonon emission in one- and two-electron QDs (artificial hydrogen and helium atoms) by electrical pump-and-probe experiments, and find that the total spin is an excellent quantum number in artificial atoms. This is attractive for potential applications to spin based information storage.

The QD we study is located in a circular pillar (diameter of 0.5 μm) fabricated from an AlGaAs/InGaAs heterostructure (see Figs. 1a and 1b)[4]. Electrons can be injected from, and collected by, the source (s) and drain (d) electrodes through asymmetric tunneling barriers, whose tunneling rates are $\Gamma_s \sim (3\ \mathrm{ns})^{-1}$ and $\Gamma_d \sim (100\ \mathrm{ns})^{-1}$ for the barrier nearest to the source and the drain, respectively. The number of electrons in the dot, N, can be controlled exactly by applying a voltage, V_g, to the surrounding gate electrode (g). Electrons are confined in an $In_{0.05}Ga_{0.95}As$ quantum well (thickness $a = 12$ nm) in the vertical (z) direction, and by a two-dimensional harmonic potential in lateral (x and y) direction appropriate for small N. The first few electrons occupy the 1s and 2p orbitals associated with the lateral confinement. Since our QD does not have circular symmetry[7,8], orbital degeneracy is lifted even at zero magnetic field, and only a two-fold spin degeneracy is expected. For this non-circular (approximately elliptic) QD, we still use 1s, 2p, ... to label the orbitals for convenience. This non-circularity does not affect much our discussion or the underlying physics. The following experiments are carried out at a temperature, T, of ~100 mK, unless otherwise stated.

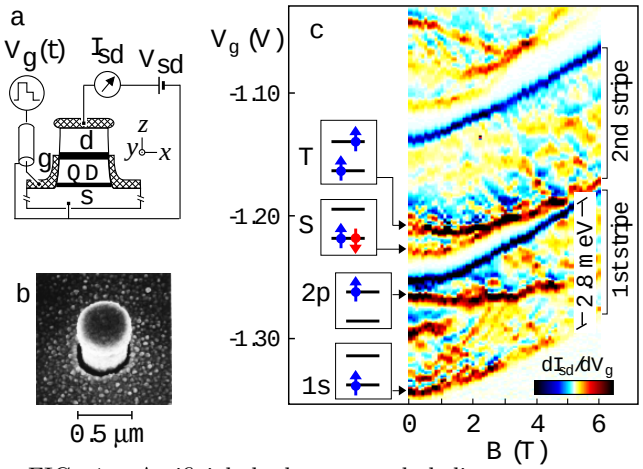

FIG. 1. Artificial hydrogen and helium atoms. **a**, Schematic set up for the pulse measurement on the vertical quantum dot. The $In_{0.05}Ga_{0.95}As$ quantum dot (QD) is connected to the source (s) and the drain (d) electrodes made of Si doped GaAs by asymmetric $Al_{0.22}Ga_{0.78}As$ tunneling barriers (7 nm thick for the lower one and 8.5 nm for the upper one. Their tunneling rates, $\Gamma_s \sim (3\ \mathrm{ns})^{-1}$ and $\Gamma_d \sim (100\ \mathrm{ns})^{-1}$, are obtained by separate measurements). The gate electrode (g) is connected to a pulse generator, which produces a gate voltage, $V_g(t)$, of rectangular or double-step shape. The measurements are performed in a dilution refrigerator in a magnetic field $B = 0$ - 5 T applied parallel to the z direction. **b**, A scanning-electron-micrograph of a control device. **c**, dI_{sd}/dV_g for the $N = 1$ and 2 QD taken with a large source-drain voltage ($V_{sd} = 2.8$ mV). The first (second) current stripe gives information about the $N = 1$ (2) QD. The peaks indicated by the arrows show the B-field evolution of the ground state (lowest edge of each stripe) and the first excited state. The relevant 1- and 2-electron configurations are also shown, in which the lower (upper) horizontal line represents 1s (2p) orbital.

First we investigate the $N = 1$ QD (artificial hydrogen), in which single electron occupies the 1s orbital (the ground state) or the 2p orbital (the first excited state). The energy spectrum of these states can be obtained by tunneling spectroscopy[5]. The current, I_{sd}, increases stepwise with increasing V_g (giving peaks in dI_{sd}/dV_g) each time an empty dot state enters the transport window. Color plot of dI_{sd}/dV_g vs V_g traces taken as a function of magnetic field (B) applied in the z direction are shown in Fig. 1c. The peak spacings within a given stripe can be related to the energy spacings between corresponding states. The energy spacing between the 1s and 2p states, ε_{1s-2p}, of the $N = 1$ QD deduced from

the first current stripe is plotted in Fig. 2e. The lateral confinement of our QD can be approximated by two orthogonal harmonic potentials in the x and y plane[7]. The characteristic confinement energies, $\hbar\omega_x \sim 2.5$ meV and $\hbar\omega_y \sim 5.5$ meV ($\hbar \equiv h/2\pi$ is the Planck's constant), are obtained by fitting ε_{1s-2p} (see solid line in Fig. 2e). The Zeeman splitting of the electron spin is small ($E_Z \sim 0.1$ meV at $B = 5$ T), and is unresolved in our experiments.

We now focus on the energy relaxation from the 2p state to the 1s state in the $N = 1$ QD, which changes the electron's orbital momentum but preserves the spin. Electrical pump-and-probe experiments are performed by applying a gate voltage of rectangular-shaped time dependence, $V_g(t)$, which switches between V_l and V_h as shown in Fig. 2a, to the gate. Experimental details are given in Refs. 9 & 10. First, the $N = 0$ QD is prepared during the low-phase of the pulse ($V_g = V_l$, see Fig. 2b). The period, t_l = 100 - 200 ns, is made sufficiently long to ensure that both the 1s and 2p states are empty. When the pulse is switched on ($V_g = V_h$, see Fig. 2c) such that only the 2p state is located in the transport window, an electron can be injected into the 2p state from the source (pump) with a time constant, $\Gamma_s^{-1} \sim 3$ ns. The electron can only escape to the drain (probe) more slowly, with a time constant, $\Gamma_d^{-1} \sim 100$ ns. However, this escape process can be interrupted by the relaxation into the 1s ground state. Thus, the current contains information about the relaxation lifetime, τ_{1s-2p}. We measure the averaged dc current, I_p, under the application of the pulse train. Figure 2d shows how this current changes with the pulse length, t_h. I_p is then converted into an average number of tunneling electrons per pulse, $\langle n_t \rangle = I_p(t_h + t_l)/e$ (e is the elementary charge). From a detailed analysis of the rate equations including all possible tunneling processes for the $N = 1$ QD, we find $\langle n_t \rangle \sim \Gamma_d \tau_{1s-2p}[1 - \exp(-t_h/\tau_{1s-2p})]$ under the condition, $\Gamma_s^{-1} \lesssim \tau_{1s-2p} < \Gamma_d^{-1}$, required for the relaxation time measurement[9]. We made sure that this condition is satisfied in all measurements for the $N = 1$ QD. The relaxation time thus estimated from the rise time of $\langle n_t \rangle$ is $\tau_{1s-2p} \sim 10$ ns for the case in Fig. 2d. The small saturation value of $\langle n_t \rangle \sim 0.02$ indicates very efficient relaxation.

We discuss the origin of the relaxation in artificial hydrogen. For an energy spacing in the meV region, and at low temperature (thermal energy $\sim$10 μeV $\ll \varepsilon_{1s-2p}$), spontaneous emission of a *phonon*, rather than a photon, dominates the relaxation process[6]. The energy spacing coincides with the acoustic-phonon energy in the linear dispersion regime. Because of the discrete energy of the states, the relaxation involves emission of a phonon of energy equal to ε_{1s-2p} (with corresponding phonon wavelength, λ_{1s-2p}). In our experiment, ε_{1s-2p}, and hence λ_{1s-2p}, vary with B as shown in Figs. 2e and 2f. Note also that the characteristic sizes l_x and l_y for the lateral dimensions of the QD decrease with increasing B. The strength of the electron-phonon interaction is expected to be suppressed for λ_{1s-2p} smaller than the characteristics size of the QD (phonon bottleneck effect[11]). Therefore, the B dependence of τ_{1s-2p} in Fig. 2g is because the phonon emission is suppressed (i.e. τ_{1s-2p} increases) with decreasing B when λ_{1s-2p} becomes shorter than a, l_x, and l_y.

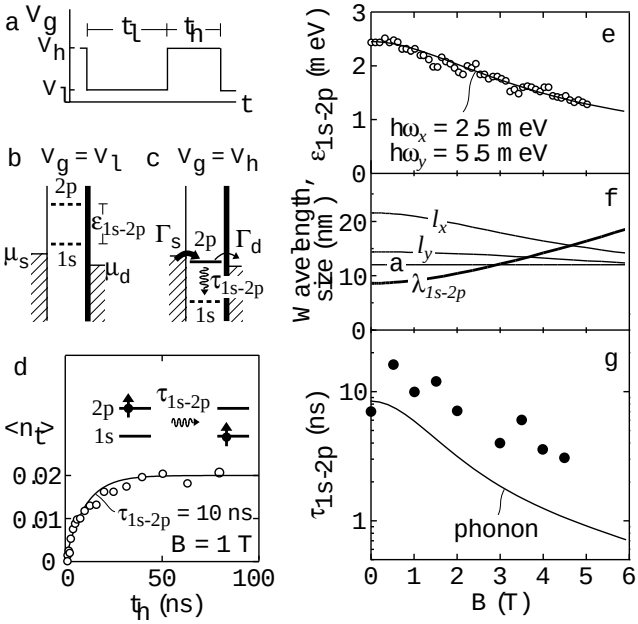

FIG. 2. Relaxation time of a one-electron QD (artificial hydrogen atom). **a**, Schematic of pulse waveform used for the electrical pump-and-probe experiment. **b** and **c**, Schematic energy diagrams along the z direction showing low and high pulse situations. The thick and thin vertical lines denote the asymmetric tunneling barriers. States in the electrodes are filled up to the Fermi energies, μ_s for the source and μ_d for the drain. The source-drain voltage, V_{sd}, opens a small transport window $eV_{sd} = \mu_s - \mu_d \sim 0.1$ meV. Solid and dashed horizontal lines denote filled and empty single-particle states, respectively. When $V_g = V_l$ **b**, the 1s and 2p states are located above μ_s and μ_d. When $V_g = V_h$ **c**, only the 2p state is located in the transport window. The 2p state is pumped from the source at a tunneling rate, $\Gamma_s \sim$ (3 ns)$^{-1}$, and probed at a slower rate, $\Gamma_d \sim$ (100 ns)$^{-1}$. The current measures the momentum relaxation time of the 2p state, τ_{1s-2p}. **d**, The average number of tunneling electrons per pulse, $\langle n_t \rangle$, measured at 1 T. The relaxation time, $\tau_{1s-2p} = 10$ ns, is obtained from the exponential curve (solid line) fitted to the data. The inset shows the electron configuration before and after relaxation. **e through g**, Magnetic field, B, dependence of **e** the energy spacing between the 2p excited state and the 1s ground state, ε_{1s-2p}, **f** the longitudinal acoustic phonon wavelength, λ, and characteristic sizes of the QD (a, l_x and l_y), and **g** the energy relaxation time, τ_{1s-2p}. In **f**, λ is calculated for the phonon at energy ε_{1s-2p} using a GaAs sound velocity of 5100 m/s. The characteristic lateral size in the x/y direction is given by $l_{x/y} = \sqrt{\hbar/m^*}(\omega_{x/y}^2 + \omega_c^2/4)^{-1/4}$, where m^* is the effective mass. The solid line in **g** is calculated for spontaneous emission of an acoustic phonon.

In order to be quantitative, we calculate the phonon emission rate from Fermi's golden rule including both deformation and piezoelectric types of coupling with standard GaAs material parameters[13,14]. For simplicity, the calculation is done for a circular dot, whose effective confinement energy is $\hbar\omega_{eff} = \hbar\sqrt{\omega_x\omega_y(1+\omega_c^2/(\omega_x+\omega_y)^2)}$, where ω_c is the cyclotron frequency. This assumption is reasonable because Coulomb interactions in an elliptic QD just scale with $\hbar\omega_{eff}$[7]. As shown by the solid line in Fig. 2g, we find good agreement with the data. The difference by about a factor of 2 or 3 might come from the assumptions about the confinement potential and uncertainties in the material parameters. Thus, the fast energy relaxation in $N = 1$ QD can be understood by spontaneous emission of a phonon. It should be noted that no clear selection rule for orbital momentum is expected, because the electron-phonon interaction cannot be approximated by a dipole interaction, and because of the anisotropic confinement potential.

In contrast, the relaxation time is remarkably different for a $N = 2$ QD (artificial helium). At low magnetic fields (see second stripe in Fig. 1c for $B < 2.5$ T), the many-body ground state is a spin-singlet (labeled S) with two antiparallel-spin electrons occupying the 1s orbital, while the first excited state is a spin-triplet (labeled T) with two parallel-spin electrons, one each occupying the 1s and 2p orbitals[4,5]. Because of direct Coulomb and exchange interactions, the energy spacing between the two states, ε_{S-T} ($\sim$0.6 meV at $B = 0$ T), is smaller than ε_{1s-2p}. Energy relaxation from the first excited state (T) to the ground state (S) not only involves the same change in orbital momentum as that in the $N = 1$ QD, but also requires a spin-flip because of Pauli exclusion (see inset of Fig. 3e). A simple phonon-emission transition from the spin-triplet to the spin-singlet is forbidden by spin conservation.

We now investigate to what degree this transition is "forbidden". The simple rectangular pulse technique employed for the $N = 1$ QD is not useful for this $N = 2$ QD transition, because the relaxation lifetime, τ_{S-T}, is always beyond the measurable range ($\tau_{S-T} > \Gamma_d^{-1} \sim$ 100 ns)[9]. Instead, we subject the QD to a double-step voltage-pulse, in which V_g is switched between three voltages, V_l, V_h and V_m as shown in Fig. 3a. First, when $V_g = V_l$ (Fig. 3b), the $N = 1$ QD is prepared during a sufficiently long period, $t_l = 100$ ns. When V_g is suddenly increased to V_h (Fig. 3c), an electron can enter to create the $N = 2$ triplet state within the interval $\sim \Gamma_s^{-1} = 3$ - 7 ns. $V_g = V_h$ for the duration $t_h = 100$ ns - 100 μs, which is much longer than Γ_s^{-1}. The triplet state may suffer a relaxation process during this time. When V_g is changed to V_m (Fig. 3d), an electron in the triplet state can tunnel out to the drain, if the triplet state is not yet relaxed to the singlet state. We set the period, $t_m = 300$ ns, to be longer than Γ_d^{-1} so we can read out the signal. We repeatedly apply the double-step pulse (effectively $\sim 10^7$ times) to obtain a reliable current I_p, and evaluate the average number of tunneling electrons, $\langle n_t\rangle = I_p(t_l + t_h + t_m)/e$. Since the current measures the unrelaxed electron number, $\langle n_t\rangle = A\exp(-t_h/\tau_{S-T})$ for the condition $\Gamma_s^{-1} \lesssim \tau_{S-T}$ (no upper limit in principle), where $A \sim 1$ is approximately the ratio of Γ_s^{-1} for the triplet to that for the singlet. Figure 3e shows a typical measurement of $\langle n_t\rangle$ at 0 T, indicating a relaxation time of $\tau_{S-T} \sim 200$ μs. This relaxation time is 4 to 5 orders of magnitude longer than that observed in the $N = 1$ QD.

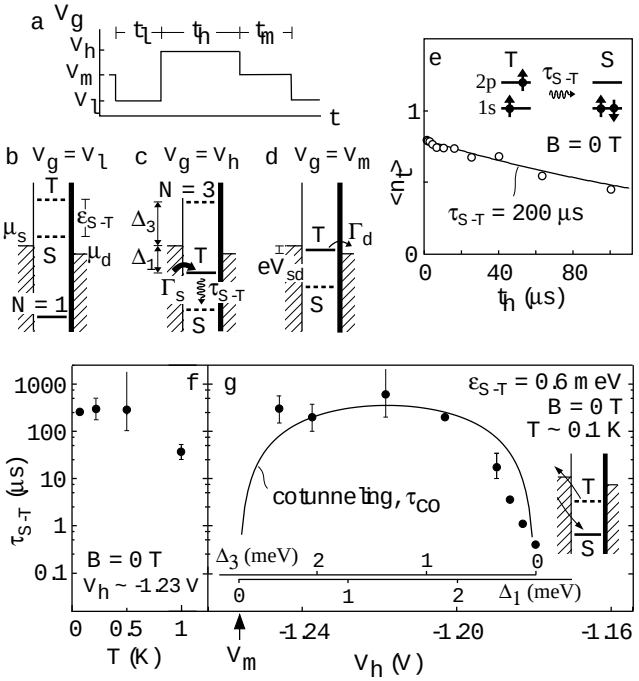

FIG. 3. Relaxation time of a two-electron QD (artificial helium atom). **a**, Schematic of double-step pulse waveform to measure extremely long relaxation times. **b through d**, Schematic energy diagram showing low, high and intermediate pulse situations. Solid and dashed horizontal lines denote filled and empty many-body states, respectively. $\mu_s - \mu_d \sim$ 0.1 meV. When $V_g = V_l$ **b**, the spin-singlet ground state S and the spin-triplet first excited state T are located above μ_s and μ_d. The system will always become the $N = 1$ QD after a sufficiently long period, $t_l = 100$ ns. When $V_g = V_h$ **c**, the QD can be excited to the triplet state within $\Gamma_s^{-1} \sim 7$ ns. The triplet state can then relax to the singlet state during the period, $t_h = 0.1$ - 100 μs. When $V_g = V_m$ **d**, the triplet state is probed by allowing an electron to tunnel into the drain. This period is fixed at $t_m = 300$ ns. **e**, Average number of tunneling electrons per pulse, $\langle n_t\rangle$ at 0 T. The relaxation time, $\tau_{S-T} = 200$ μs, is obtained from the exponential decay (solid line). The inset shows the electron configuration before and after relaxation. **f**, Temperature, T, dependence of the relaxation time τ_{S-T} at 0 T. **g**, The gate voltage, V_h, dependence of τ_{S-T}. V_h is also converted into Δ_1 and Δ_3 energy scales. Δ_1 and Δ_3 are indicated in **c**. The solid line is calculated for cotunneling processes. The inset shows a schematic of these inelastic cotunneling processes.

We find no clear B dependence of τ_{S-T} (always longer than 100 μs), at least for the energy spacings between 0.6 meV at $B = 0$ T and 0.24 meV at $B = 2$ T (not shown). We also investigate the temperature dependence of τ_{S-T} (Fig. 3f). No clear change is observed up to 0.5 K. τ_{S-T} decreases above 0.5 K, where thermal excitation from the QD to the electrodes becomes important.

On the other hand, we do find that τ_{S-T} strongly depends on the high gate-pulse voltage V_h, during which relaxation takes place, as shown in Fig. 3g. Although V_h is swept deep into the $N = 2$ Coulomb blockade region (-1.27 V $< V_g <$ -1.16 V), τ_{S-T} decreases rapidly at $V_h \sim$ -1.18 V. This V_h dependence implies a strong influence of the source and drain electrodes. Even though the Coulomb blockade is robust in the suppression of transport, higher-order tunneling processes can contribute to the relaxation and change τ_{S-T}. An electron in the dot can be replaced with an electron of opposite spin from the electrodes (see inset of Fig. 3g). This results in energy loss in the QD, whereas the electrode gains the same energy. This inelastic cotunneling rate, τ_{co}^{-1}, is estimated by considering second-order tunneling processes[15–17]. For the relaxation mechanisms considered here, the $N = 2$ QD can relax virtually through $N = 1$ or $N = 3$ intermediate states. Note that this process does not cause a net current even at a finite voltage of $e|V_{sd}| < \varepsilon_{S-T}$[18]. Assuming $V_{sd} = 0$ V and zero temperature for simplicity, we obtain $\tau_{co}^{-1} = \varepsilon_{S-T}(\hbar\Gamma_s + \hbar\Gamma_d)^2(\Delta_1^{-1} + \Delta_3^{-1})^2/h$. Here, Δ_1 and Δ_3, respectively are the energies required to excite the initial $N = 2$ triplet state to the $N = 1$ and 3 intermediate states, as indicated in Fig. 3c. We can extract Δ_1 and Δ_3 from V_h, and the values are shown in Fig. 3g. The solid line shows τ_{co}, the relaxation time due to cotunneling, calculated with experimentally deduced parameters ($\varepsilon_{S-T} = 0.6$ meV, and $(\Gamma_s + \Gamma_d)^{-1} =$ 7 ns). Clearly the observed relaxation time can be well understood by inelastic cotunneling.

Our observations for $N = 1$ and 2 QDs can be compared with real atoms[1]. The transition from the 2p state to the 1s state in atomic hydrogen is allowed by photon emission (the Lyman α transition line), while that in artificial hydrogen is allowed by *phonon* emission. The transition from the spin-triplet state to the spin-singlet state is forbidden by conservation of the total spin for both atomic helium and artificial helium. Moreover, these "forbidden" transitions can occur by collisions with electrons for the helium atom, and by cotunneling for the $N = 2$ QD. Spin conservation also applies to any transition in light atoms, and probably likewise to few-electron QDs. The difference between the allowed and forbidden transitions leads to more than 11 orders of magnitude difference in the relaxation times for real hydrogen and helium atoms. Our observation of 4 to 5 orders of magnitude difference in our $N = 1$ and 2 artificial atoms is not as high, but is still surprisingly large. Note that this difference would become larger if cotunneling in QDs can be suppressed by using thicker tunneling barriers. Very importantly, the large difference between τ_{1s-2p} and τ_{S-T} originates from the fact that other effects, such as spin-orbit and hyperfine interactions[19,20], must have only a weak effect on the breaking of the "forbidden" symmetries. We now discuss how small these hidden contributions are by focusing on the spin-orbit interactions.

Spin-orbit interactions are predicted to give the dominant contribution to spin relaxation in GaAs QD systems[20], although this is still an extremely small effect. For simplicity, we consider the spin-orbit interaction energy, Δ_{so}, only for coupling between the 1s and 2p orbitals, but including all effects which mix spin and orbital degrees of freedom. Simple perturbation theory[21] predicts that the relaxation time from the triplet to the singlet is given by $\tau_{S-T,so} \sim (\varepsilon_{S-T}/\Delta_{so})^2\tau_{phonon}(\varepsilon_{S-T})$. Here, $\tau_{phonon}^{-1}(\varepsilon_{S-T})$ is the phonon emission rate at the phonon energy, ε_{S-T}, and we know that τ_{phonon} is well accounted for by the electron-phonon interaction. Therefore, we can deduce an upper bound of $\Delta_{so} < 4$ μeV from our observations ($\tau_{S-T} > 200$ μs). This value is close to the spin-orbit induced spin splitting energy ($\sim$ 2.5 μeV) observed in a GaAs two-dimensional electron gas system[22]. Note that spin-orbit interactions are significantly enhanced in nanoparticles, e.g. copper, probably because of impurities or interfaces[21], but our vertical semiconductor QD are largely free of these undesirable factors.

Our experiments indicate that the spin degree of freedom in QDs is well isolated from the orbital degree of freedom. This is particularly attractive for applications to spin memories and spin quantum bits (qubits)[23,24]. For a simple scheme involving just a single-electron spin in a magnetic field, the spin-orbit interactions can degrade the energy relaxation time (T_1) of a spin qubit. We estimate the dominant contribution, $T_{1,so}$, using a perturbative approach, $T_{1,so} \sim (\varepsilon_{1s-2p}/\Delta_{so})^2\tau_{phonon}(\varepsilon_Z)$. Since $\Delta_{so} < 4$ μeV, this yields $T_{1,so} > 1$ ms for a Zeeman splitting $\varepsilon_Z \sim 0.1$ meV and $\varepsilon_{1s-2p} \sim 1.2$ meV at $B \sim 5$ T ($T_{1,so} > 100$ μs at $B \sim 9$ T). This $T_{1,so}$ is thus comparable to that obtained by electron-spin-resonance for donor states in GaAs[25], and is much longer than the time required for typical one- and two-qubit operations[26]. Note that small spin-orbit interactions are also desirable with respect to the dephasing time (T_2) of a spin qubit[27]. Our results therefore encourage further research in the use of the spin degree of freedom in QDs.

[1] Bethe, H. A., & Salpeter, E. E., *Quantum Mechanics of One- and Two-Electron Atoms*, (Springer, Berlin, 1957).

[2] Kouwenhoven, L. P. *et al.*, in *Mesoscopic Electron Transport* (eds Sohn, L. L., Kouwenhoven, L. P. & Schön, G.) 105-214 (NATO ASI series E 345, Kluwer, Dordrecht, 1997).

[3] Ashoori, R. C. *et al.*, Single-electron capacitance spec-

troscopy of discrete quantum levels. *Phys. Rev. Lett.* **68**, 3088 (1992).
[4] Tarucha, S., Austing, D. G., Honda, T., van der Hage, R. J. & Kouwenhoven, L. P., Shell filling and spin effects in a few electron quantum dot. *Phys. Rev. Lett.* **77**, 3613 (1996).
[5] Kouwenhoven, L. P. *et al.*, Excitation spectra of circular, few-electron quantum dots. *Science* **278**, 1788 (1997).
[6] Fujisawa, T. *et al.*, Spontaneous emission spectrum in double quantum dot devices. *Science* **282**, 932 (1998).
[7] Tokura, Y., Sasaki, S., Austing, D. G. & Tarucha, S., Excitation spectra and exchange interactions in circular and elliptical quantum dots. *Physica B* **298**, 260 (2001).
[8] Matagne, P., Leburton, J. P., Austing, D. G. & Tarucha, S., Shell charging and spin-filling sequences in realistic vertical quantum dots. *Phys. Rev. B* **65**, 085325 (2002).
[9] Fujisawa, T., Tokura, Y. & Hirayama, Y., Transient current spectroscopy of a quantum dot in the Coulomb blockade regime. *Phys. Rev. B* **63**, 081304 (2001).
[10] Fujisawa, T., Austing, D. G., Tokura, Y., Hirayama, Y. & S. Tarucha, Non-equilibrium transport through a vertical quantum dot in the absence of spin-flip energy relaxation. *cond-mat/0204314*.
[11] Benisty, H., Sotomayer-Torres, C. M. & Weisbuch, C., Intrinsic mechanism for the poor luminescence properties of quantum-box systems. *Phys. Rev. B* **44**, 10945 (1991).
[12] Bockelmann, U. *et al.*, Time resolved spectroscopy of single quantum dots: Fermi gas of excitons?. *Phys. Rev. Lett.* **76**, 3622 (1996).
[13] Seeger, K., *Semiconductor Physics: An Introduction* 153-213 (Springer-Verlag, Berlin, 1985).
[14] Bockelmann, U., Phonon scattering between zero-dimensional electronic states: Spatial versus Landau quantization. *Phys. Rev. B* **50**, 17271 (1994).
[15] Averin, D. V. & Nazarov, Yu. V., in *Single Charge Tunneling: Coulomb Blockade Phenomena in Nanostructures* (eds Grabert, H. & Devoret, M. H.) 217-247 (Plenum Press and NATO Scientific Affairs Division, New York, 1992).
[16] Eto, M., Electronic states and transport phenomena in quantum dot systems. *Jpn. J. Appl. Phys.* part 1 **40**, 1929 (2001).
[17] Sukhorukov, E. V., Burkard, G. & Loss, D., *Phys. Rev. B* **63**, 125315 (2001).
[18] De Franceschi, S. *et al.*, Electron cotunneling in a semiconductor quantum dot. *Phys. Rev. Lett.* **86**, 878 (2001).
[19] Pikus, G. E. & Titkov, A. N., in *Optical Orientation* (eds Meier, F. & Zakharchenya, B. P.) 73-131 (Elsevier, Amsterdam, 1984).
[20] Khaetskii, A. V. & Nazarov, Yu. V., Spin relaxation in semiconductor quantum dots. *Phys. Rev. B* **61**, 12639 (2000).
[21] Halperin, W. P., Quantum size effects in metal particles. *Rev. Mod. Phys.* **58**, 533 (1986).
[22] Bychkov, Yu. A. & Rashba, E. I., Properties of a 2D electron gas with lifted spectral degeneracy. *JETP Lett.* **39**, 78 (1984).
[23] Loss, D. & DiVincenzo, D. P., Quantum computation with quantum dots. *Phys. Rev. A* **57**, 120 (1998).
[24] Recher, P., Sukhorukov, E. V. & Loss, D., Quantum dot as spin filter and spin memory, *Phys. Rev. Lett.* **85**, 1962-1965 (2000).
[25] Seck, M., Potemski, M. & Wyder, P., High-field spin resonance of weakly bound electrons in GaAs. *Phys. Rev. B* **56**, 7422 (1997).
[26] Gupta, J. A., Knobel, R., Samarth, N. & Awschalom, D. D., Ultrafast manipulation of electron spin coherence. *Science* **292**, 2458 (2001).
[27] Kavokin, K. V., Anisotropic exchange interaction of localized conduction-band electrons in semiconductors. *Phys. Rev. B* **64**, 075305 (2001).

Acknowledgement

We thank G. E. W. Bauer, T. Honda, T. Inoshita, A. V. Khaetskii, L. P. Kouwenhoven for discussions and help.

Correspondence and requests for materials should be addressed to T.F. (e-mail: fujisawa@will.brl.ntt.co.jp).